

Residual Stress and Deformation Modelling for Metal Additive Manufacturing Processes

Heng Liu, Todd Sparks, Frank Liou

Missouri University of Science and Technology/ Department of Mechanical Engineering
Rolla MO 65409, USA
liou@mst.edu

David M. Dietrich

Missouri University of Science and Technology/ Department of Systems Engineering
Rolla MO 65409, USA

Abstract –Metal additive Manufacturing has gained increasing attention in the area of rapid manufacturing and repairing. This process involves extremely high thermal gradients and heat and cooling rate, resulting in residual stresses and distortion. This paper presents a 3D sequentially coupled thermo-mechanical finite element model to predict residual stresses and deformations. The temperature distribution, thermal stress field and geometry deformation across domain are illustrated. The effect of deposition parameters on residual stress and deflections are also explored. A set of validation experiments for mechanical effects were conducted using laser displacement sensor. The comparisons between the simulated and experimental results show good agreement.

Keywords: Residual stress, deformation, additive manufacturing, finite element analysis, experimental validation

1. Introduction

Highly localized heating and cooling during direct metal deposition (DMD) process may produce nonuniform thermal expansion and contraction, resulting in complicated distribution of residual stresses in the heat affect zone and unexpected distortion in the whole structures as shown in Fig. 1. The residual stresses may promote fracture and fatigue and induce unpredictable buckling during the service of deposited parts and the distortion is often detrimental to the dimensional accuracies of structures. Therefore, it is vital to predict the behaviour of materials after DMD process and optimize the design/manufacturing parameters to control the residual stresses and distortion.



Fig. 1. A metal deposition process may produce nonuniform thermal expansion and contraction, resulting in distribution of residual stresses in the heat affect zone.

The focus of this paper is to investigate both the thermal and mechanical behaviour of DMD process of Stainless Steel 304. Based on finite element analysis package ABAQUS, a 3-D sequentially coupled

thermo-mechanical model is developed to simulate the transient temperature field, residual stress and final deformation. A laser displacement sensor is used to record the deflection of the substrate caused by thermal stresses during the deposition process. By comparing experiment results with simulation results, the numerical model is validated.

2. Residual Stress and Distortion

Residual stresses are those stresses that would exist in a body if all external loads were removed. When a material is heated uniformly, it expands uniformly and no thermal stress is produced. But when the material is heated unevenly, thermal stress is produced (Masubuchi, 1980). Highly localized heating and cooling during the DMD process produces non-uniform thermal expansion and contraction, which results in a complicated distribution of residual stresses in the heat affect zone and unexpected distortion across the entire structure. The residual stresses may promote fractures and fatigue and induce unpredictable buckling during the service of deposited parts. This distortion often is detrimental to the dimensional accuracies of structures; therefore, it is vital to predict the behaviour of materials after the DMD process and to optimize the design/manufacturing parameters in order to control the residual stresses and distortion.

3. Overall Simulation and Experiment Approach

Based on the finite element (FE) analysis package ABAQUS, a 3-D, sequentially coupled, thermo-mechanical model was developed to simulate the transient temperature field, residual stress and final deformation involved in the DMD process. The numerical modelling involved two main steps and the solution processes are shown in Fig. 2. In the first step, a transient thermal analysis was carried out to generate the temperature history of the entire work piece. In the second step, mechanical analysis was conducted to calculate the residual stress and deformation of work piece, and the load for this step is the temperature field file generated in previous step.

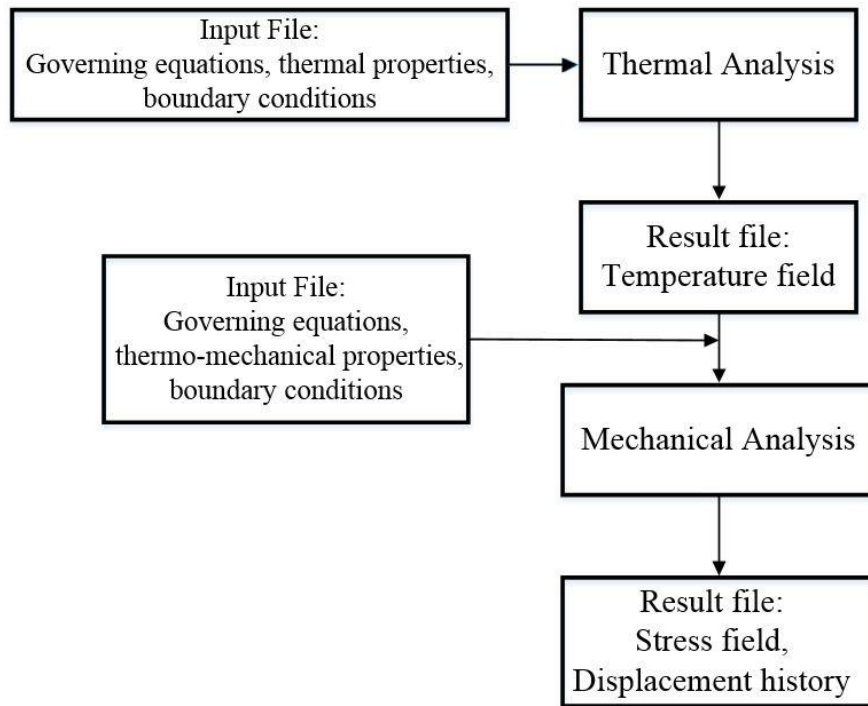


Fig. 2. Flow Chart Showing the Process of Numerical Modelling

In order to validate the case study, an experiment was conducted by using a laser displacement sensor to record the deflection of the substrate caused by thermal stresses during the deposition process. By comparing the experimental results with simulation results, the numerical model was validated. This validated model can be extended to multi-layer laser aided DMD process of stainless steel under various process parameters and further to other materials.

4. Finite Element Modelling Of Residual Strss and Distorsion

4. 1. Governing Equations

In the DMD process, the stress/deformation field in a structure would largely depend on the temperature field, but the influence of the stress/deformation field on the temperature field is negligible. Thus, a heat transfer analysis not coupled with mechanical effect is considered.

The transient temperature field $T(x, y, z, t)$ throughout the domain was obtained by solving the 3-D heat conduction equation, Eq. (1), in the substrate, along with the appropriate initial and boundary conditions (Reddy, 2010).

$$\rho C \frac{\partial T}{\partial t} = \frac{\partial}{\partial x} \left(k \frac{\partial T}{\partial x} \right) + \frac{\partial}{\partial y} \left(k \frac{\partial T}{\partial y} \right) + \frac{\partial}{\partial z} \left(k \frac{\partial T}{\partial z} \right) + Q \quad (1)$$

Where T is the temperature, ρ is the density, C is the specific heat, k is the heat conductivity, and Q is the internal heat generation per unit volume. All material properties were considered temperature-dependent.

4. 2. Initial and Boundary Conditions

The initial conditions applied to solve Eq. (1) were:

$$T(x, y, z, 0) = T_0 \quad (2)$$

$$T(x, y, z, \infty) = T_0 \quad (3)$$

Where T_0 is the ambient temperature. In this study, T_0 was set as room temperature, $298.15 K$. The boundary conditions including thermal convection and radiation, are described by Newton's law of cooling and the Stefan-Boltzmann law, respectively. The internal heat source term, Q in Eq. (1), also was considered in the boundary conditions as a surface heat source (moving laser beam). The boundary conditions then could be expressed as (Reddy, 2010):

$$K(\Delta T \cdot \mathbf{n})|_{\Gamma} = \begin{cases} \left[-h_c(T - T_0) - \varepsilon\sigma(T^4 - T_0^4) \right] |_{\Gamma} & \Gamma \notin \Lambda \\ \left[Q - h_c(T - T_0) - \varepsilon\sigma(T^4 - T_0^4) \right] |_{\Gamma} & \Gamma \in \Lambda \end{cases} \quad (4)$$

where k , T , T_0 and Q bear their previous definitions, \mathbf{n} is the normal vector of the surface, h_c is the heat convection coefficient, ε is the emissivity which is 0.9 in the case study as described in Section 5 of this paper, σ is the Stefan-Boltzman constant which is $5.6704 \times 10^{-8} W/m^2K^4$, Γ represents the surfaces of the work piece and Λ represents the surface area irradiated by the laser beam.

4. 3. Adjustments and Assumptions

Accurate modelling of the thermal process results in highly nonlinear coupled equations. To simplify the solution process and reduce the computational cost, the following adjustments and assumptions were considered.

4. 3. 1. Energy Distribution of the Laser Beam

In the experiment, a circular shaped laser beam shot onto the substrate vertically with a constant and uniform power density. Thus, the heat source term Q in Eq. (1) was considered a constant and uniformly distributed surface heat flux defined as:

$$Q = \frac{\alpha P}{\pi r^2} \quad (5)$$

Where α is the absorption coefficient, P is the power of the continuous laser, and r is the radius of the laser beam. In the case study, α was set as 0.4 according to numerous experimental results, and $r = 1.25 \text{ mm}$.

4. 3. 2. Movement of Laser Beam

The motion of the laser beam was taken into account by updating the position of the beam's center R with time t as follows:

$$R = \left[\left(x - \int_{t_0}^t u dt \right) + \left(y - \int_{t_0}^t v dt \right) + \left(z - \int_{t_0}^t w dt \right) \right]^{\frac{1}{2}} \quad (6)$$

where x , y , and z are the spatial coordinate the laser beam center, u , v , and w are the continuous velocities the laser beam travels along x , y , and z direction.

4. 3. 3. Powder Addition

In modelling, the continuous powder addition process is divided into many small time steps. Using the "Model Change" (Simulia, 2011), in each time step, a set of elements was added onto the substrate to form rectangular deposits along the centerline of the substrate. The width of the deposits was assumed to be the same as the diameter of the laser beam, and the thickness of the deposits was calculated from the speed at which the laser travelled and the powder feed rate with an efficiency of 0.3 in the case study. The geometry of the deposits was updated at the end of each step to simulate corresponding boundary conditions.

4. 3. 4. Latent Heat of Fusion

The effect of the latent heat of fusion during the melting/solidification process was accounted for by modifying the specific heat. The equivalent specific heat c_p^* is expressed as (Toyserkani et al., 2004):

$$c_p^*(T) = c_p(T) + \frac{L}{T_m - T_0} \quad (6)$$

Where $c_p^*(T)$ is the modified specific heat, $c_p(T)$ is the original temperature-dependent specific heat, L is the latent heat of fusion, T_m is the melting temperature, and T_0 is the ambient temperature. In

the case study, the values of the latent heat of fusion, solidus temperature and liquidus temperature of SS 304 (Ghosh, 2006) appear in Table 1.

Table. 1. Latent Heat of Fusion for Stainless Steel 304

Latent Heat of Fusion (J/kg)	Solidus Temperature (K)	Liquidus Temperature (K)
273790	1703	1733

4. 3. 5. Marangoni Effect

The effect of Marangoni flow caused by the thermocapillary phenomenon significantly impacts the temperature distribution so it must be considered in order to obtain an accurate thermal field solution (Alimardani et al., 2007). Based on the method proposed by Lampa et al. (Lampa et al., 1997), artificial thermal conductivity was used to account for the Marangoni effect:

$$k_m(T) = \begin{cases} k(T) & T \leq T_{liq} \\ 2.5 \cdot k(T) & T > T_{liq} \end{cases} \quad (7)$$

Where $k_m(T)$ is the modified thermal conductivity, T_{liq} is the liquidus temperature, and T and $k(T)$ maintain their previous definitions.

4. 3. 6. Combined Boundary Conditions

The boundary conditions shown in Eq. 4 can be rewritten as:

$$K(\Delta T \cdot \mathbf{n})|_{\Gamma} = \begin{cases} [(-h_c - h_r)(T - T_0)]|_{\Gamma} & \Gamma \notin \Lambda \\ [Q - (-h_c - h_r)(T - T_0)]|_{\Gamma} & \Gamma \in \Lambda \end{cases} \quad (8)$$

Where h_r is the radiation coefficient expressed as:

$$h_r = \varepsilon \sigma (T^2 + T_0^2)(T + T_0) \quad (9)$$

Eq. (8) indicates that convection was dominant at low temperatures, while radiation made a major contribution to heat loss at high temperatures. Because Eq. (9) is a 3rd-order function of temperature T , a highly nonlinear term was introduced by the radiation coefficient, thus greatly increasing the computational expense. Based on experimental data, an empirical formula combining convective and radiative heat transfer was given by Vinokurov (1977) as:

$$h = h_c + \varepsilon \sigma (T^2 + T_0^2)(T + T_0) \approx 2.41 \times 10^{-3} \varepsilon T^{1.61} \quad (10)$$

Where h is the combined heat transfer coefficient which is a lower order function of temperature T compared with h_r . The associated loss in accuracy using this relationship is estimated to be less than 5% (Labudovic and Kovacevic, 2003). In ABAQUS, a user subroutine "FILM" is written to simulate heat loss as follows:

SUBROUTINE FILM(H,SINK,TEMP,KSTEP,KINC,TIME,NOEL,NPT,

```

1 COORDS, JLTY, FIELD, NFIELD, SNAME, NODE, AREA)
INCLUDE 'ABA_PARAM.INC'
DIMENSION H(2),TIME(2),COORDS(3),FIELD(NFIELD)
CHARACTER*80 SNAME

SINK=298.15                ! Sink temperature
H(1)=0.002169*(TEMP**1.61) ! Film coefficient
H(2)=0.0034921*(TEMP**0.61) ! Rate of change of the film coefficient
30 RETURN
40 CONTINUE
END

```

4. 3. 7. Material Properties

Temperature-dependent thermal physical properties, including density, specific heat, thermal conductivity and latent heat, should be used as inputs.

4. 3. 8. Element Selection

The type and size of elements used to approximate the domain were determined on the basis of computational accuracy and cost. In transient heat transfer analysis with second-order elements, there is a minimum required time increment. A simple guideline is (Simulia, 2011):

$$\Delta t > \frac{6c}{\rho k} \Delta l^2 \quad (11)$$

Where c , ρ and k are as previously defined, Δt is the time increment, and Δl is a typical element dimension. If the time increment is smaller than this value, nonphysical oscillations may appear in the solution. Such oscillations are eliminated with first-order elements (Simulia, 2011) but can lead to inaccurate solutions (Reddy, 2010). Considering the stability along with the computational time and accuracy, first-order 3-D heat transfer elements (C3D8) with h-version mesh refinement (refine the mesh by subdividing existing elements into more elements of the same order) were used for the case study. Fine meshes were used in the deposition zone, and the mesh size gradually increased with the distance from the deposits. In regions more separated from the heat affect zone, coarser meshes were utilized.

5. Case Study

A clamped cantilever beam when deposit material in the middle of the beam as shown in Fig. 3 is used an example here. 14496 elements were created due to numerical convergence within 1% error to model this case.

The residual stress distribution within the final deposits is shown in Fig. 4 (a quarter of deposits is hidden to show internal residual stress). Normal stresses σ_{11} , σ_{22} , σ_{33} along three spatial directions are shown in Fig. 4(a)-4(c) respectively and the Von Mises stress is shown in Fig. 4(d). It can be seen that compressive residual stress exists in the top free surface of deposits. This is caused by the steep temperature gradient. The temperature gradient in x and y direction can be as high as 450 K/mm and 1400 K/mm respectively. The expansion of hotter top layer is inhibited by underlying material, thus introducing compressive stress in top surface. Residual stresses in lower part of deposits are mostly tensile stresses due to cool-down phase of the molten layers (Merzelis and Kruth, 2006). After the deposition is finished and laser is turned off, the remelted lower part of deposits begin to shrink and this shrinkage is restricted by the underling material, thus tensile stresses are induced.

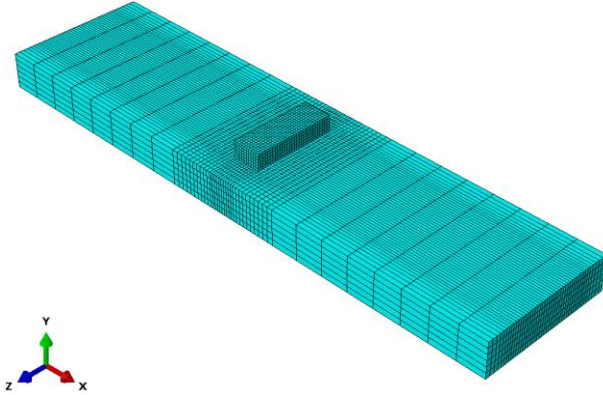


Fig. 3. The meshing scheme of a clamped cantilever beam when deposit material in the middle of the beam.

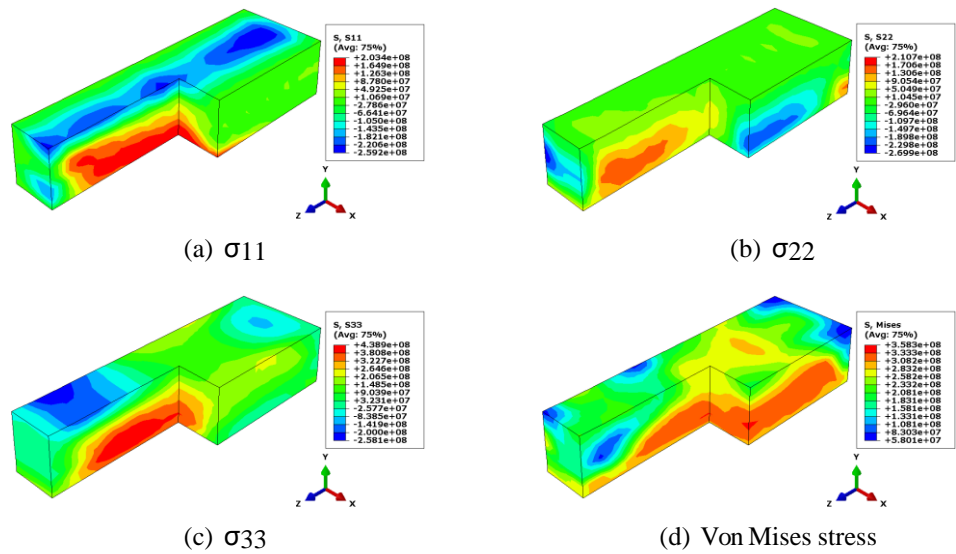


Fig. 4. Contour plots of residual stress field within deposits

During DMD process, the substrate will continuously experience expansion and shrinkage and finally keep a deformed shape. In this paper, deflection in y direction, shown in Fig. 5, is the main deformation under consideration and is observed by both experiments and simulations shown below.

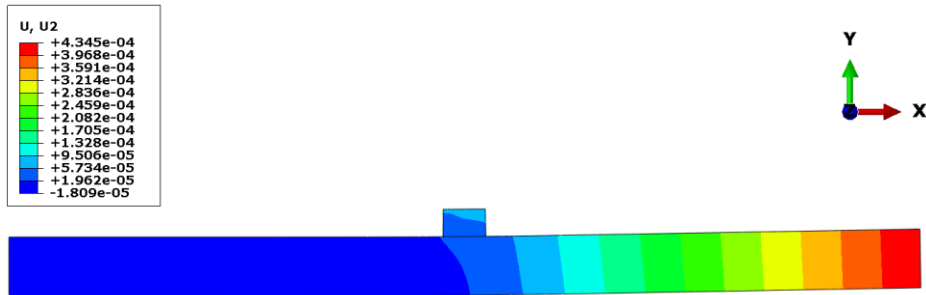


Fig. 5. Deflection of substrate in y direction

An experimental validation was also conducted. The substrate is clamped at the left end to prevent rigid body motion as shown in Fig 5. Keyence's LK-G5000 series laser displacement sensor is put right below the right end of the substrate to record the displacement of the free end in y direction with frequency of 25 Hz during the process. The experimental setup is shown in Fig 6. Fig. 7 shows the comparisons of deflection of substrate between experiment and simulation results for both cases. It can be seen from these plots that the trend of the deflection calculated from the simulation matches very well with the experiment results. For each deposition layer, the substrate firstly bends down due to thermal expansion on the top surface and then bends up due to thermal shrinkage during the cooling process. After completely cooled down, the substrate keeps the deformed shape.

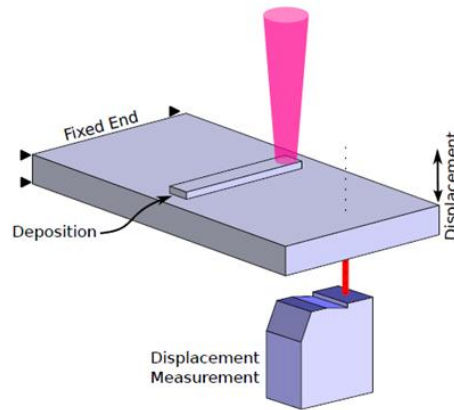
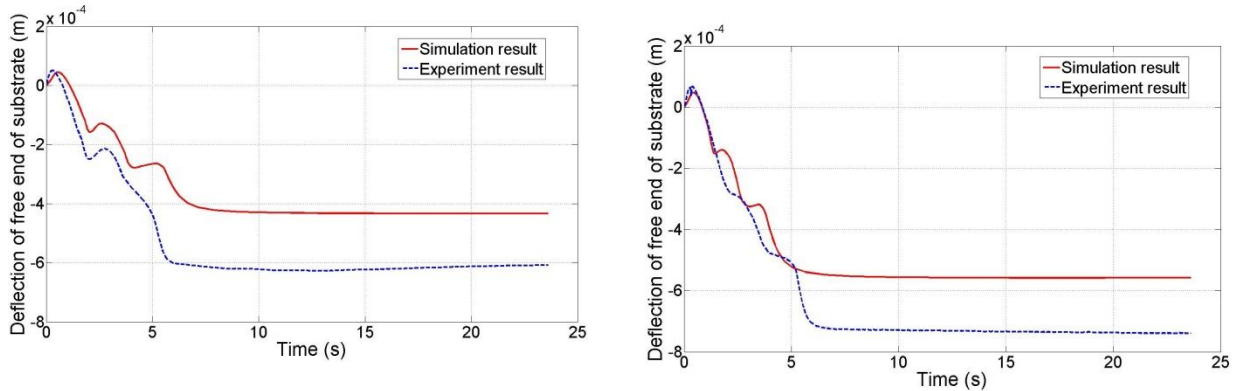


Fig. 6. Experimental Setup



(a) Deflection in Case 1

(b) Deflection in Case 2

Fig. 7. Simulation and experiment results of deflection of substrate

The differences of final deflection value between simulation and experiment are 28.5% and 24.6% for case 1 and 2 respectively. There are several reasons could be responsible for these differences. Firstly, errors exist in experiment set up. In the simulation, laser beam travels exactly along the centerline of substrate. However, this cannot be perfectly accomplished in experiments. These offsets would affect the deflection to a large extent since the deflection is sensitive to the position of heated zone and measuring point.

Secondly, the laser displacement sensor does not track the displacement of one particular node. It works by sensing the signal reflected by obstacle so the positions it monitors is always changing as the substrate keeps deforming. The simplifications and assumptions considered in both thermal and mechanical analysis are also important factors contributing to the differences.

6. Conclusion

A sequentially coupled thermo-mechanical finite element model is developed and validated by experiment. The results show the characteristics of temperature distribution, residual stress and deformation within formed deposits and substrates. Finite Element modelling can be used to predict the resulting mechanical behaviour of materials after DMD processes effectively. More efforts are needed to explore more complicated situations in industry and to optimize design/manufacturing parameters to control the residual stress and distortion.

Acknowledgements

This work was partially funded through NASA's Fundamental Aeronautics Program, Fixed Wing Project, under NRA NNX11AI73A, Boeing, and Rolls Royce. The authors would like to acknowledge William J. Seufzer and Karen Taminger of NASA Langley Research Center for their critical advice and mentorship. Support from Missouri S&T's Intelligent Systems Center, Material Research Center, and Manufacturing Engineering program is also greatly appreciated.

References

- Alimardani, M., Toyserkani, E., & Huissoon, J. P. (2007). A 3D Dynamic Numerical Approach For Temperature And Thermal Stress Distributions In Multilayer Laser Solid Freeform Fabrication Process. *Optics and Lasers in Engineering*, 45(12), 1115-1130.
- Ghosh, S. (2006). *Process Modeling for Solidification Microstructure and Transient Thermal Stresses in Laser Aided DMD Process*. Unpublished Doctor of Philosophy, University of Missouri--Rolla.
- Labudovic, M., Hu, D., & Kovacevic, R. (2003). A Three Dimensional Model For Direct Laser Metal Powder Deposition And Rapid Prototyping. *Journal Of Materials Science*, 38(1), 35-49.
- Lampa, C., Kaplan, A. F., Powell, J., & Magnusson, C. (1997). An Analytical Thermodynamic Model Of Laser Welding. *Journal of Physics D: Applied Physics*, 30(9), 1293-1299.
- Liou, F. (2008). *Rapid Prototyping and Engineering Applications: A Toolbox for Prototype Development* (Dekker Mechanical Engineering). CRC Press, 2008, ISBN-10: 0849334098, ISBN-13: 978-0849334092.
- Heng, L., Sparks, T. E., Liou, F., Dietrich, D. M. (2013). Numerical Analysis of Thermal Stress and Deflection in Multi-Layer Laser Metal Deposition Processes. *Proceedings of the 24th Solid Freeform Fabrication Symposium*.
- Masubuchi, K. (1980). *Analysis Of Welded Structures: Residual Stresses, Distortion, And Their Consequences*. Oxford, United Kingdom: Pergamon press.
- Mercelis, P., & Kruth, J. (2006). Residual Stresses In Selective Laser Sintering And Selective Laser Melting. *Rapid Prototyping Journal*, 12(5), 254-265.
- Reddy, J. N., & Gartling, D. K. (2010). *The finite element method in heat transfer and fluid dynamics*, CRC Press LLC, Boca Raton, FL
- Simulia, D. (2011). *ABAQUS 6.11 Analysis User's Manual.*, 22-2.
- Toyserkani, E., Khajepour, A., & Corbin, S. (2004). 3-D Finite Element Modeling Of Laser Cladding By Powder Injection: Effects Of Laser Pulse Shaping On The Process. *Optics and Lasers in Engineering*, 41(6), 849-867.
- Vinokurov, V. A. (1977). *Welding Stresses and Distortion: Determination and Elimination*. British Library Lending Division.